JOURNAL OF MAGNETIC RESONANCE, Series A **118,** 84–93 (1996)
ARTICLE NO. 0012

Applications of the Bloch–Siegert Shift in Solid-State Proton-Dipolar-Decoupled ^{19}F MAS NMR

STEPHANIE A. VIERKÖTTER*

Chemical and Analytical Sciences Division, Oak Ridge National Laboratory, Oak Ridge, Tennessee 37831-6201

Received May 10, 1995; revised October 5, 1995

In solid-state proton-dipolar-decoupled ^{19}F MAS NMR spectroscopy, ^{19}F chemical-shift data need to be corrected for the Bloch–Siegert shift. Assigning the single sharp ^{19}F resonance of 2-fluoroadamantane to its proton-coupled ^{19}F shift of −174.4 ppm results in chemical-shift referencing that is independent of the amplitude of the proton-decoupling field. The Bloch–Siegert shift is also a useful tool to characterize the amplitude and homogeneity of the proton-decoupling field, H_{1H}, and to monitor probe performance. Considerable inhomogeneity in H_{1H} along the long axis of the right-cylinder sample rotor was detected. In our commercial 7 mm H–F MAS probe, the proton field strength, $\gamma_H H_{1H}$, decreases to 25% of the maximum value across the usable sample volume. Measurement of the Bloch–Siegert shift revealed that the proton-decoupling field strength decreases during the first few scans of an acquisition. Reductions in the proton field strengths can exceed 10%, and they are explained by the heating of the RF coil circuitry which is caused by high-power proton decoupling. The extent of reduction in field amplitude is a function of the decoupling duty cycle. Losses in $\gamma_H H_{1H}$ can be avoided by tuning the probe proton RF circuitry at the operating temperature of the probe, using the Bloch–Siegert shift as an optimization parameter. © 1996 Academic Press, Inc.

INTRODUCTION

It is well known that the resonance frequency of a nucleus, ν_0, shifts when a second, off-resonance RF field is applied (*1, 2*). This effect, the Bloch–Siegert shift, is a contribution to H_0 that arises from the off-resonance component of the oscillating RF irradiation field (*3*). In the context of this work, the second irradiation field is a heteronuclear dipolar decoupling field, hereafter referred to as the ''decoupling field,'' H_1. The effect is manifested as a shift in the Larmor frequencies of the observed nuclei. For the off-resonance case where the difference between the Larmor frequencies of the decoupled and the observed nuclei is much larger than the frequency of the decoupling field, $|\omega - \omega_0| \gg \omega_1$, the Bloch–Siegert shift, Δ, is described by (*4*)

$$\Delta = \frac{(\gamma_{\text{obs}} H_1)^2}{\omega_0^2 - \omega^2}, \qquad [1]$$

where γ_{obs} is the gyromagnetic ratio of the observed nucleus, H_1 is the decoupling field in gauss, ω_0 is the Larmor frequency of the observed nucleus, and ω is the Larmor frequency of the decoupled nucleus. Reference (*2*) gives the Bloch–Siegert shift for the off-resonance case as $\omega_1^2/(\omega_0^2 - \omega^2)$. The examples given on p. 227 in this reference show that ω_1 is taken as γH_1 with γ as the gyromagnetic ratio of the *decoupled* nucleus. This was found to give Bloch–Siegert shifts which are too large compared to shifts measured by Webb and Zilm (*4*) and ourselves. Correct values are obtained when γ is taken as the gyromagnetic ratio of the *observed* nucleus. Using the gyromagnetic ratio of the observed nucleus makes sense since the Bloch–Siegert shift expresses the interaction between the H_1 field and the field of the moment of the observed nucleus. By use of the relationships $\omega = 2\pi\nu$ and $\gamma = \gamma/(2\pi)$, Eq. [1] can be written as

$$\Delta = \frac{(\gamma_{\text{obs}} H_1)^2}{\nu_0^2 - \nu^2}. \qquad [2]$$

Equations [1] and [2] show that the Bloch–Siegert shift is proportional to the square of the decoupling field, H_1, and inversely proportional to the difference between the squared Larmor frequencies of the observed and the decoupled nuclei. The amplitude of the proton decoupling field, in hertz, is calculated by multiplying H_1 (gauss) from Eq. [2] by γ of the proton nucleus, i.e., $\gamma_H H_{1H}$.

In $\{^1H\}^{13}C$ NMR spectroscopy of liquids or dissolved solids, where the proton decoupling field H_{1H} serves to remove scalar coupling, the required decoupling-field strengths are relatively small, e.g., 10 kHz. For this decoupling field, the Bloch–Siegert shift is very small, 6.7×10^{-4} ppm at a static magnetic field, H_0, of 2.35 T (see Table 1). In solid-state proton-dipolar-decoupled ^{13}C, $[^1H]^{13}C$, MAS NMR spectroscopy, the ^{1}H decoupling fields employed are typi-

---

* Current address: Department of Chemistry, Louisiana State University, Baton Rouge, Louisiana 70803-1804.

1064-1858/96 $12.00

TABLE 1

Magnitudes of the Bloch–Siegert shift in Proton-Decoupled Carbon and Fluorine NMR Spectroscopy for Different Proton-Decoupling Amplitudes, $\gamma_H H_{1H}$, and Different Static Magnetic-Field Strengths, H_0

	H_0 (T)	$\gamma_H H_{1H}$ (kHz)	Δ (ppm)
$\{^1H\}^{13}C$	2.35	10	6.7×10^{-4}
$[^1H]^{13}C$	2.35	100	6.7×10^{-2}
$[^1H]^{19}F$	2.35	50	1.9
	2.35	100	7.7
	1.41	100	21.4

Note. $\{^1H\}$ designates proton decoupling in solution NMR (removal of scalar coupling only), and $[^1H]$ stands for dipolar proton decoupling as applied in solid-state NMR experiments.

cally 50–70 kHz since such field strengths are necessary to remove the heteronuclear C–H dipolar interactions. Even for a 100 kHz proton decoupling field, the Bloch–Siegert shift in $[^1H]^{13}C$ NMR is only 6.7×10^{-2} ppm (1.7 Hz).

In solid-state ^1H-dipolar-decoupled ^{19}F, $[^1H]^{19}F$, MAS NMR spectroscopy, the difference between the Larmor frequencies of the observed and decoupled nuclei is 6 MHz at 2.35 T (rather than 75 MHz as in the case of proton-decoupled ^{13}C NMR), and large Bloch–Siegert shifts are observed. In $[^1H]^{19}F$ NMR spectroscopy at 2.35 T, a proton decoupling field of 50 kHz leads to a shift of 1.9 ppm (181 Hz) and a decoupling field of 100 kHz produces a shift of 7.7 ppm (725 Hz; Table 1). It is apparent that valid comparisons of ^{19}F chemical shifts measured in the solid state in the presence of proton decoupling are possible only if the reported values are independent of the amplitude of the proton decoupling field. The correction for the Bloch–Siegert shift becomes even more important at lower static magnetic fields, H_0, where the Bloch–Siegert shift is larger (Eqs. [1] and [2]). At 1.41 T (60 MHz ^1H Larmor frequency), the Bloch–Siegert shift in a $[^1H]^{19}F$ NMR experiment using a 100 kHz decoupling field is 21.4 ppm (1209 Hz; Table 1).

In this paper, the Bloch–Siegert shifts observed in solid-state $[^1H]^{19}F$ NMR spectroscopy are discussed from several perspectives: (1) a method for correcting solid-state ^{19}F chemical shifts for the Bloch–Siegert shift is reported; (2) H_{1H} field amplitudes are determined from the measurement of the Bloch–Siegert shift; (3) the observation of the Bloch–Siegert shift is used to evaluate the homogeneity (*4, 5*) of the proton-decoupling field throughout the sample volume; (4) the inhomogeneity in H_{1H} across the sample is used to observe the sublimation of 2-fluoroadamantane, **1,** within the sample rotor; (5) heating of the RF coil circuitry by application of proton decoupling and its influence on the measurement of the Bloch–Siegert shift are discussed; and (6) a procedure for tuning the proton RF coil circuitry under actual measurement conditions using the Bloch–Siegert shift is described.

EXPERIMENTAL

General

^{19}F solid-state NMR experiments with and without proton decoupling were performed on a Bruker MSL-100 spectrometer using a H–F double-tuned probe that allows magic-angle spinning speeds up to 7–8 kHz (Doty Scientific Inc.). The right-cylinder sample rotor is placed inside of the double-tuned, four-turn RF coil (105 nH). The coil is made from gold-plated Cu foil (5 μm Au) and is 13.2 mm long. The copper foil is 1.7 mm in width. The coil is wrapped such that the gap between the start and the end points of the foil for the first turn is 0.5 mm, 1.85 mm for the second and third turns, and 0.5 mm for the forth turn. The coil is wrapped about the stator which has an o.d. of 8.25 mm. The right-cylinder sample rotors are made from zirconia or silicon nitride and have an outer diameter of 7.0 mm and a length of 22.1 mm. Maximum sample volume (about 360 μl) is achieved with use of two short end caps that leave 16.1 mm of length of the rotor for the sample. Several experiments described in this paper employed smaller sample volumes. In these cases, the remaining volume was taken up by spacers made from boron nitride. The NMR experiments involve a ^{19}F Bloch-decay pulse sequence with or without proton decoupling. A 3.3 μs ^{19}F excitation pulse was used. Acquisition times were 10 ms unless cited otherwise. The recycle delay was 4 s. The magic-angle spinning speed was 4 kHz for the experiments shown in Figs. 2, 3, and 6 and 6.3 kHz for the spectra presented in Figs. 1 and 5. Digital resolution was 6 Hz.

2-Fluoroadamantane, **1,** was prepared from 2-hydroxyadamantane (Aldrich) via a procedure similar to that described by Olah *et al.* (*6*). Five grams of 2-hydroxyadamantane in ether/hexane were added dropwise to 30 ml of HF-pyridine (70/30) at 0°C. After the addition was completed, the reaction mixture was stirred at room temperature for two hours. The mixture was poured onto tossed ice and the aqueous layers were extracted with ether. The combined organic layers were washed twice with 50 ml of 10% Na_2CO_3 solution and with water. After drying over $MgSO_4$, the organic phase was concentrated and the material was purified by column chromatography (neutral alumina in hexane). A total weight of 3.1 g of pure 2-fluoroadamantane was obtained. Alternatively, **1** can be prepared from 2-hydroxyadamantane by reaction with diethylaminosulfur trifluoride (DAST) as reported by Adcock (*7*).

Chemical-Shift Referencing

Chemical-shift referencing in $[^1H]^{19}F$ NMR experiments was achieved by blending 2-fluoroadamantane, **1** (structure shown on the right in Fig. 1), into the sample of interest. The chemical shift of **1** was set to −174.4 ppm {$\delta(\mathrm{CFCl_3}) = 0$ ppm} which corresponds to the ^{19}F chemical-shift value of this compound in solution ($\mathrm{CDCl_3}$) (*8*) in the absence of ^{1}H decoupling, i.e., in the absence of a Bloch–Siegert shift. 2-Fluoroadamantane can be easily removed from precious samples by room-temperature sublimation.

Measurements of the Proton Field Amplitude

2-Fluoroadamantane, **1,** was used neat or mixed into a sample uniformly. The Bloch–Siegert shift, measured as the difference in the chemical shifts of the proton-coupled and the proton-decoupled ^{19}F resonances, gives the proton field $H_{1\mathrm{H}}$ by Eq. [1] or [2]. $H_{1\mathrm{H}}$ (gauss) is multiplied by $\bar{\gamma}_{\mathrm{H}} = \gamma_{\mathrm{H}}/(2\pi)$ to obtain the proton field amplitude, $\bar{\gamma}_{\mathrm{H}}H_{1\mathrm{H}}$.

H_{1H} Homogeneity Measurements

For the measurement of the profile of the $H_{1\mathrm{H}}$ field (*5*) along the long axis of the rotor, boron nitride spacers were used to hold a thin sample slice, a right-cylinder volume, 0.38 ± 0.03 mm thick, in place, with the sample disk face orthogonal to the rotor axis. The Bloch–Siegert shift was measured for 11 different positions (see Figs. 3 and 4) of this slice of **1** along the axis of the rotor.

For the evaluation of radial $H_{1\mathrm{H}}$ homogeneity, the volume of the middle sample slice and an end sample slice were subdivided further into an annulus of sample (i.d. = 2.7 mm, o.d. = 5.4 mm) and an on-axis inner core (o.d. = 2.7 mm), again using boron nitride spacers. The Bloch–Siegert shifts that arise from **1** packed in these two volumes (annulus and inner core) were compared.

Measurement of the Sublimation Behavior of **1**

2-Fluoroadamantane, **1,** 3.8 wt%, was blended with 3-fluoro-4-methoxybenzoic acid, **2,** to give a uniform physical mixture. The powder mixture was hand packed in a rotor, filling the entire volume that is available when using short end caps. [^{1}H]^{19}F spectra were recorded as a function of time. Each spectrum was acquired with 300 transients. At the end of this experiment, the sublimation of **1** was confirmed by visual inspection of the sample.

Heating of the RF Coil Circuitry through Proton Decoupling

Heating of the RF coil circuitry caused by proton decoupling was studied (a) by observing the Bloch–Siegert shift for a range of proton-decoupling duty cycles (proton-decoupling pulses of 2.5 to 40.5 ms width with a recycle delay of 4 s) and (b) by measuring the Bloch–Siegert shift for a given proton-decoupling pulse width (20.5 ms, recycle delay 4 s) as a function of the number of transients. Experiment (b) was performed using buffered acquisition so that all data could be acquired in a single experiment.

To test whether the ^{19}F chemical shift of **1** is temperature dependent, a 20.5 ms heating pulse (proton-decoupling field, 112 kHz) was applied on the proton RF channel prior to the ^{19}F excitation pulse. The excitation pulse was followed by acquisition of the fluorine signal in the absence of proton decoupling. The chemical shift of **1** measured in this experiment was compared to the proton-coupled ^{19}F shift that was recorded without any prior RF heating pulses.

Tuning and Matching of the ^{1}H RF Coil Circuitry under Measurement Conditions

A rotor packed with **1** in the middle third of the rotor volume (cf. Fig. 2d) was used in this procedure. The spectrometer was programmed to continuously record one scan of a proton-decoupled ^{19}F spectrum of this sample, to automatically process the FID, and to display the frequency of the fluorine resonance. The tuning and matching capacitors for the proton RF circuitry were adjusted to maximize the Bloch–Siegert shift of the observed fluorine resonance of **1.** This experiment was performed under conditions identical to those intended for use in the actual measurements following sample change (same recycle delay and acquisition time, same RF filters in the proton RF line, etc.). The ^{19}F RF channel was tuned and matched in the conventional, off-line manner which involves sending a low-power fluorine signal into the circuit and adjusting the tune and match for the least amount of reflected power. The tuning and matching of the proton and fluorine channels were performed in an iterative manner.

RESULTS AND DISCUSSION

(a) Chemical-Shift Referencing

The differences in the Bloch–Siegert shifts of all resonances in a given solid-state proton-dipolar-decoupled ^{19}F MAS NMR spectrum are small. For fluorine resonances separated by 20 kHz (212.3 ppm at 2.35 T), the difference is only 2.4 Hz for a proton-decoupling field amplitude, $\bar{\gamma}_{\mathrm{H}}H_{1\mathrm{H}}$, of 100 kHz. Thus, correct chemical shifts can be obtained by simply referencing one of the resonances in the proton-decoupled ^{19}F spectrum using its known proton-*coupled* chemical-shift value. This referencing procedure leads to ^{19}F chemical shifts that correspond to the values that would be measured in the absence of proton decoupling. These chemical shifts are automatically corrected for the Bloch–Siegert shift and can be compared between different investigators without knowledge of the proton-decoupling field strengths employed. A convenient way to accomplish this experiment is to blend **1** into the sample of interest to get a uniform physical mixture and set its ^{19}F resonance to −174.4 ppm,

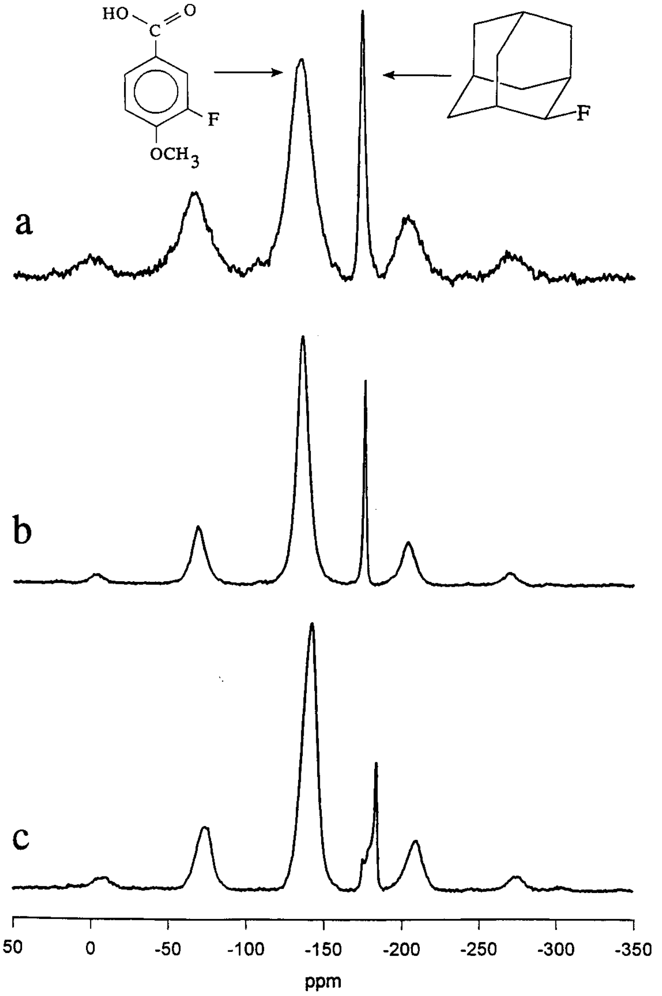

FIG. 1. Solid-state ^{19}F MAS NMR spectra of 3.8 wt% of 2-fluoroadamantane (−174.4 ppm) mixed with 3-fluoro-4-methoxybenzoic acid (−133.2 ppm) to give a uniform physical mixture. (a) ^{1}H coupled; (b, c) with $\gamma_H H_{1H}$ = 54.2 and 110.4 kHz, respectively. The magic-angle spinning rate is 6.3 kHz.

i.e., the chemical shift observed in solution ($CDCl_3$) (*8*) when no proton decoupling is employed. One advantage of using **1** as a reference compound is its relatively narrow ^{19}F resonance (for sample slice in middle of rotor: 460 Hz linewidth at half-height without ^{1}H decoupling, 90 Hz with 126 kHz $\gamma_H H_{1H}$; slice is 0.38 ± 0.03 mm thick; see under Experimental). The narrow resonance is the result of the high molecular-reorientation rate of this substance in the solid state which reduces heteronuclear dipolar interactions by motional averaging. Thus, the resonance of this compound does not obscure a large portion of the spectral window. The chemical shift of **1** can be set with higher accuracy than the shifts of typical, more rigid ^{19}F-containing compounds that give rise to resonances with linewidths at half-height of a kilohertz or more.

Figure 1 shows the solid-state ^{19}F MAS NMR spectrum for 3-fluoro-4-methoxybenzoic acid, **2,** mixed with **1** (3.8 wt%) recorded without proton decoupling (Fig. 1a) and with proton decoupling using fields of 54.2 kHz (Fig. 1b) and 110.4 kHz (Fig. 1c). The ^{1}H-coupled spectrum shows the sharp ^{19}F resonance of **1** at −174.4 ppm and a much broader resonance ($\nu_{1/2}$ = 1.5 kHz) for **2** at −133.2 ppm. The fluorine in **2** is attached to an aromatic carbon, a bonding configuration that produces a highly anisotropic electron density about the fluorine atom. This is manifested as a large chemical-shift anisotropy which gives rise to two sets of spinning side bands at a MAS speed of 6.3 kHz (*9*). The ^{1}H-decoupled spectra show that all ^{19}F resonances are shifted upfield by the same amount with respect to their chemical shifts in the ^{1}H-coupled spectrum. This shift increases with increasing proton-decoupling field strength (Figs. 1b and 1c). By setting the ^{19}F resonance of **1** in the proton-decoupled spectra to −174.4 ppm, the chemical shifts in the spectra shown in Figs. 1b and 1c become independent of the strength of the proton-decoupling field.

The asymmetry that is seen in the lineshape of **1** (Fig. 1c; see also Fig. 2c) is caused by a nonuniform proton-decoupling field which produces differential Bloch–Siegert shifts in different volume elements within the RF coil. This field inhomogeneity and its impact on chemical-shift referencing are discussed in detail in part (c) of this section.

(b) Characterization of the Amplitude of the H_{1H} Field

The measurement of the Bloch–Siegert shift is useful for a rapid characterization of the H_{1H} field amplitude and provides an alternative to the use of an external antenna which monitors the forward and reflected power of the RF. A few weight percent of **1** is blended into the sample of interest to give a uniform physical mixture, and the chemical shift of the ^{19}F resonance of the reference is measured with and without proton decoupling. The Bloch–Siegert shifts observed for the relatively sharp ^{19}F resonances of **1** in connection with Eq. [2] give the proton field H_{1H}. The field amplitude is obtained by multiplying H_{1H} by γ_H. The precision of this determination depends on the digital resolution of the measurement and on the amplitude of the decoupling field. A digital resolution of 6 Hz gives a maximum uncertainty in $\gamma_H H_{1H}$ of ±0.8 kHz (±1.6%) for a 50 kHz field and ±0.4 kHz (±0.4%) for a 100 kHz field. The citation of $\gamma_H H_{1H}$ to higher precision is not warranted since the inhomogeneity in the H_{1H} field exceeds these ranges, except for highly spatially constrained samples, as shown in the next section.

(c) Characterization of H_{1H} Field Homogeneity

Figure 2 shows expansions of ^{19}F spectra of **1** (full rotor, short end caps) recorded with (a) no proton decoupling and

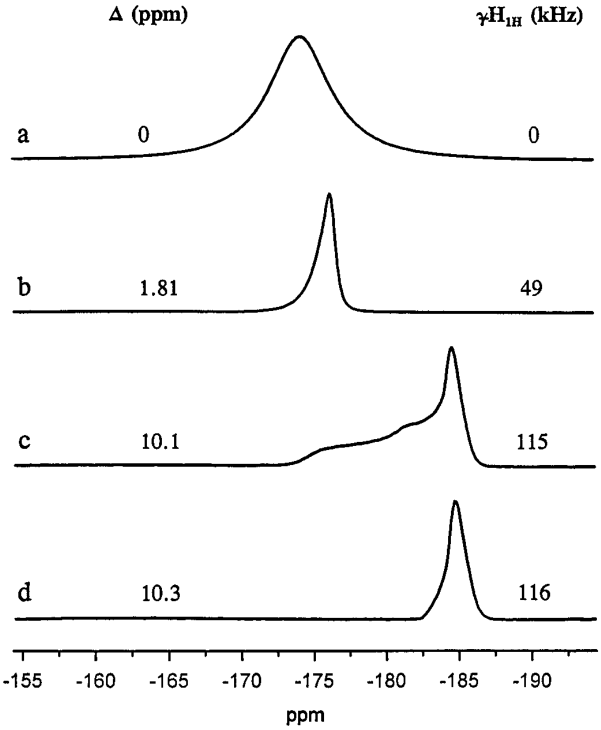

FIG. 2. Solid-state ^{19}F MAS NMR spectra of **1** (a) ^{1}H coupled and (b–d) ^{1}H decoupled as indicated. Spectra (a–c) were recorded with **1** packed into the entire rotor volume (using short end caps). Spectrum (d) is obtained from **1** restricted to the middle third (on long axis of rotor) of the rotor volume.

(b) proton decoupling of 49 kHz, and (c) 115 kHz. In the absence of proton decoupling, the full width at half-height, $\nu_{1/2}$, of the ^{19}F resonance is 460 Hz (Fig. 2a). This linewidth decreases when proton decoupling is employed (*10*) (Fig. 2b). The ^{19}F signal is strikingly asymmetric in experiments using high proton-decoupling fields (Fig. 2c). The increase in asymmetry and overall width of the signal upon increase in proton-decoupling field amplitude indicates that the $H_{1\mathrm{H}}$ field is not homogeneous throughout the sample volume. Inhomogeneity in $H_{1\mathrm{H}}$ causes the sample in different locations in the rotor to experience different Bloch–Siegert shifts, leading to the observed asymmetric lineshape.

The inhomogeneity along the long axis of the rotor was investigated by packing a 0.38 ± 0.03 mm thick disk of **1** in the sample rotor with the sample disk face orthogonal to the rotor axis. The remainder of the volume in the rotor was filled with boron nitride spacers. This sample slice was moved incrementally to 11 different positions in the rotor, and the Bloch–Siegert shift was measured. The result of this experiment using a proton-decoupling field strength of 127 kHz is shown in Figs. 3 and 4. Figure 3 presents the spectra obtained from the 11 slices of **1.** The positions of these slices within the rotor are indicated in Fig. 4. Slice 6 is in the middle of the rotor while slices 1 and 11 are positioned at opposite ends of the sample rotor using short end caps (see under Experimental). The spectra of **1** in slices 5, 6, and 7 (Fig. 3) in the center of the rotor show the largest Bloch–Siegert shifts, Δ, and the highest signal-to-noise-ratios. The Δ values of these slices correspond to $\gamma_{\mathrm{H}}H_{1\mathrm{H}}$ of 125, 126, and 127 kHz, respectively. Slices of **1** that were positioned further removed from the center of the rotor show a drastic decrease both in their Bloch–Siegert shifts and in their signal-to-noise ratios. Slices 1 and 11 give rise to such poor signal sensitivity that the number of scans for these spectra was increased 8- and 23-fold, respectively.

The data from Fig. 3 are plotted in Fig. 4 as the proton field strength, $\gamma_{\mathrm{H}}H_{1\mathrm{H}}$, calculated from the measured Δ, versus the positions of the sample slices along the long axis of the rotor. The graph shows that the $H_{1\mathrm{H}}$ field along the long axis of the rotor drops off drastically toward either end of the rotor. The maximum field strength, $\gamma_{\mathrm{H}}H_{1\mathrm{H}\,\mathrm{max}}$, of 127 kHz near the center of the rotor is reduced to about 32 kHz at

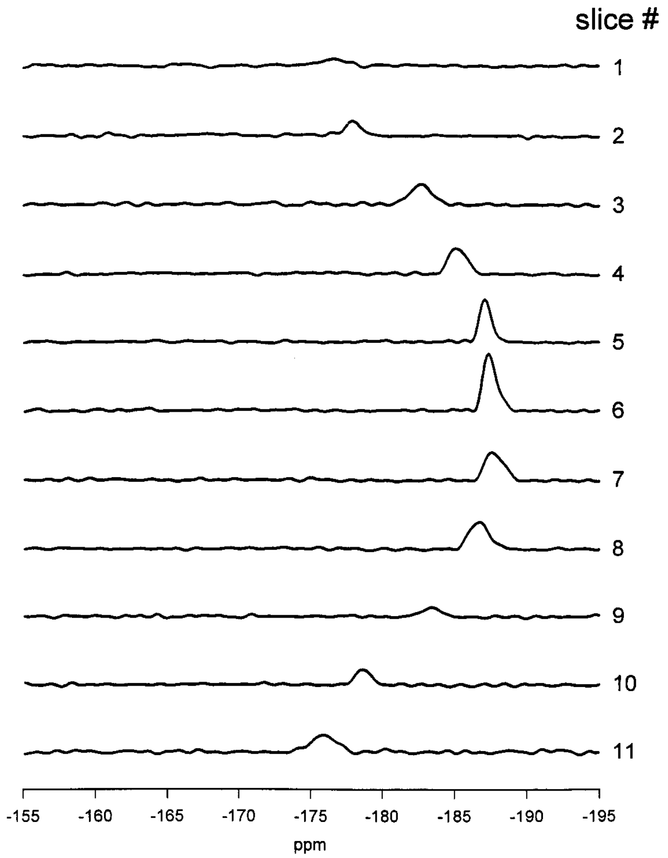

FIG. 3. Solid-state [^{1}H]^{19}F MAS NMR spectra of **1** packed as a thin disk, 0.38 ± 0.03 mm thick, with the sample disk face orthogonal to the rotor's long axis. The 11 spectra are derived from this sample slice being placed in 11 different positions within the rotor as indicated in Fig. 4. The maximum $\gamma_{\mathrm{H}}\mathrm{H}_{1\mathrm{H}}$ is 127 kHz (slice 7).

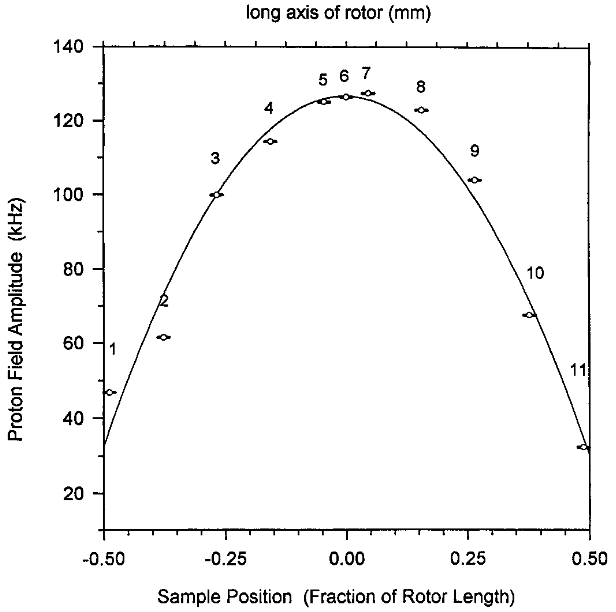

FIG. 4. Profile of the proton field amplitude, $\gamma_H H_{1H}$, along the long rotor axis. The plot is based on the data shown in Fig. 3. The *x* axis shows the 11 positions of the sample disk along the rotor's long axis in fractions of the rotor length (the length refers to the usable rotor length, i.e., excluding the portion that is taken up by the short end caps). Zero on the lower *x* axis indicates the midpoint of the rotor axis. The upper *x* axis is marked off in millimeters. The horizontal line drawn through each data point represents the thickness of the sample disk, 0.38 ± 0.03 mm.

the ends of the rotor. This is a reduction to 25% of $\gamma_H H_{1H\,\max}$. The data in Fig. 4 indicate that only about 40% of the rotor volume centered about the position of slice 7 (0.7 mm offset from the middle of the rotor) may be filled with sample if the decrease in H_{1H} field amplitude across the sample should not exceed 10% of $\gamma_H H_{1H\,\max}$. If an H_{1H} homogeneity of 20% is acceptable, 60% of the rotor volume may be filled with sample. The slight deviation of the data points from the quadratic function in Fig. 4 shows that the reduction of the H_{1H} field amplitude is not quite symmetrical about $\gamma_H H_{1H\,\max}$. The slice experiment shown in Figs. 3 and 4 was repeated for lower proton-decoupling fields with maximum field amplitudes of 56 and 94 kHz (data not shown). The decrease in $\gamma_H H_{1H}$, in percent of the maximum, is about the same in each case as for the example shown in Figs. 3 and 4 (the amplitude drops from the maximum at slice 7 to 52–53% of the maximum value at slice 10 in all cases).

Figure 2d shows the proton-decoupled ^{19}F MAS spectrum of a sample of **1** which was constrained to the middle third of the rotor volume (using BN spacers) rather than being packed in the entire rotor volume (Fig. 2c). The comparison of Figs. 2c and 2d clearly shows the improvement in H_{1H} homogeneity upon using a significantly reduced rotor volume centered within the rotor. These spectra were recorded with the same proton-decoupling field strength. The Bloch–Siegert shifts measured using the peak maxima in Figs. 2c and 2d give field strengths of 115 and 116 kHz, respectively, i.e., values that agree within 1%. Consequently, it is not necessary to restrict **1** to the center of the rotor to get an accurate measure of $\gamma_H H_{1H\,\max}$. Instead, **1** may be mixed uniformly with the sample and the Bloch–Siegert shift determined using the frequency of the 2-fluoroadamantane resonance at highest peak intensity.

The H_{1F} field will show the same inhomogeneity over the rotor volume as H_{1H}. A ^{19}F excitation pulse that leads to a 90° rotation for those spins in the center of the rotor generates a 23° rotation for ^{19}F spins at the rotor ends. The latter ^{19}F spins give rise only to 40% of their integrated intensity in the spectrum, relative to that observed using a 90° pulse excitation (Fig. 2c). Despite this underrepresentation, the H_{1H} inhomogeneity in **1** is visible as an asymmetric, heterogeneously broadened signal. This observation of H_{1H} inhomogeneity in [^{1}H]^{19}F MAS spectra by lineshape analysis is exceptional since most fluorine resonances are broad enough ($\nu_{1/2} \geqslant 1$ kHz) to obscure this effect (see the spectrum of **2** in Fig. 1). Differential Bloch–Siegert shifts for samples packed in the entire rotor volume become visible when the ^{19}F linewidth is exceptionally narrow. This situation applies for compounds with high degrees of mobility, e.g., **1,** and for large monofluorinated molecules that have slow ^{19}F–^{19}F spin diffusion.

Radial inhomogeneity in the H_{1H} field was also investigated. For this purpose, the Bloch–Siegert shift was remeasured for thin slices of **1** in the center and at one end of the rotor (slices 6 and 1) as described above, except in this experiment each of these sample slices was subdivided further into an annulus and an inner core of sample (see under Experimental). It was found that the sample in annulus and inner core of slice 6 exhibited equal Bloch–Siegert shifts to within 1%. Thus, radial inhomogeneity in H_{1H} at the center of the rotor (coil) is negligible. However, when this experiment was repeated for slice 1, marked differences in the Bloch–Siegert shifts for **1** in the annulus and in the inner core were observed. The H_{1H} field amplitude found in the annulus is weaker than in the core by about a factor of two, indicating that radial inhomogeneity is dramatic for the sample at the rotor ends.

While a detailed profile of the radial inhomogeneity has not been measured, these experiments show that radial inhomogeneity is increasingly significant as the sample location is further removed from the center of the rotor (coil). The linewidths in the spectra of the 11 sample slices of **1** (Fig. 3) could be indicative of the extent of radial inhomogeneity at those 11 positions along the long axis of the rotor. However, these linewidths are not influenced solely by radial inhomogeneity but also by axial inhomogeneity since the sample slices are of finite thickness and the drop in field strength across the slice thickness is much more drastic for slices close to the end caps than for those near the center of the rotor (Fig. 4). A minor error contribution to the linewidths is the uncertainty in the reproducibility of the sample slice thickness for the 11 slice positions (see under Experimental).

Figure 2d shows that packing the sample in the middle third of the rotor volume results in a more homogeneous $H_{1\mathrm{H}}$ field over the sample dimensions. The ^{19}F spectrum does not show the characteristic low-field asymmetry seen in Figs. 1c and 2c. Restricting the sample to a fraction of the rotor volume centered about the middle of the rotor significantly reduces both axial and radial inhomogeneities. Uniformly blending **1** into the sample has the advantage of providing both the minimum and the maximum $\gamma_{\mathrm{H}}H_{1\mathrm{H}}$ over the sample volume in experiments performed with large decoupling fields (see Fig. 1c). This method allows one to determine rapidly the minimum and maximum proton field strengths over the chosen sample volume with one experiment instead of having to perform a more tedious study involving several samples slices as shown in Figs. 3 and 4.

Close inspection of the ^{19}F lineshape of **1** recorded with high proton-decoupling power (Figs. 1c, 2c, and 5a) reveals that two portions of the downfield ''tail'' of the lineshape have somewhat higher intensities than the remainder of the tail. As discussed above, the width of the lineshape indicates the spread in proton-decoupling field strengths across the sample. The intensities of the individual resonances that lead to the observed lineshape are proportional to the amount of sample that experiences a given field strength, and they are also weighted by the $H_{1\mathrm{F}}$ field profile across the sample. To accurately account for the detail of the lineshape including the fine structure, several additional factors must be taken into account. The spinning of the sample often causes some repacking of the sample within the rotor, leading to small cone-shaped voids near the ends of the rotor. Higher resolution in the profile of the proton-decoupling field strength across the long axis of the sample might reveal ripples in the profile that correspond to the gaps between the turns of the coil. Furthermore, the radial inhomogeneity needs to be considered to predict the lineshape correctly in detail. The detailed simulation of the lineshape is, however, not necessary for the determination of the strength and the inhomogeneity of the H_1 field. This information is readily extracted from the observed lineshapes as described above.

(d) Sublimation Behavior of 1 *within the Rotor in Long-Term Experiments*

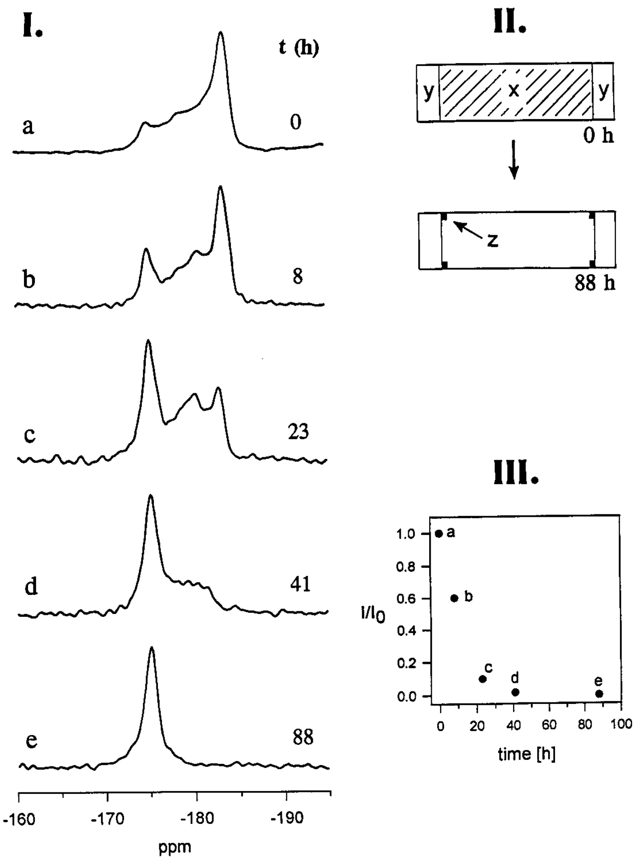

FIG. 5. (I) [^{1}H]^{19}F MAS NMR spectra of 3.8 wt% of **1** uniformly blended into **2**, recorded as a function of time ($\gamma_{\mathrm{H}}H_{1\mathrm{H\,max}}$ = 110.4 kHz; MAS rate = 6.3 kHz). Only the signals of **1** are shown. Each spectrum represents 300 scans. (II) Cross section of the rotor. In the beginning of the experiment, the concentration of **1** is constant throughout the sample volume *x* (*y* indicates the rotor end caps). After 88 h, **1** has accumulated at the ends of the rotor (*z*). (III) The ratio of I/I_0, i.e., the intensity of the fluorine resonance at −183.8 ppm (resonance with highest peak intensity in Ia) at time *t* over the initial intensity of this resonance, versus the experimental evolution time.

The inhomogeneity in $H_{1\mathrm{H}}$ that was discussed in the previous section has a surprising consequence in experiments using **1** as a chemical-shift reference in long-term experiments. Figure 5 (I) shows the ^{19}F signals of **1** in the proton-decoupled ^{19}F MAS spectra of a uniform physical mixture of **1** (3.8 wt%) and **2** as a function of time. In the beginning of the experiment, the asymmetric lineshape is indicative of **1,** being distributed evenly throughout the rotor volume (cf. Fig. 2c). The ^{19}F resonance of the highest peak intensity in Fig. 5 (I.a) at −183.8 ppm exhibits a Bloch–Siegert shift of 9.4 ppm corresponding to a value for $\gamma_{\mathrm{H}}H_{1\mathrm{H\,max}}$ of 110.4 kHz. Over time, the intensity of this resonance decreases (Fig. 5, I and III) as a narrow ($\nu_{1/2}$ = 140 Hz) resonance with a symmetric lineshape at −175.2 ppm grows in intensity. Eventually, all resonance area is represented in this line. This chemical shift corresponds to a Bloch–Siegert shift of only 0.8 ppm, i.e., a proton field amplitude of 32 kHz. This field amplitude represents only about 30% of the value that was measured in the beginning of the experiment. The spectra in Fig. 5 reveal that **1** physically moves toward the ends of the rotor where it accumulates. The movement of **1** occurs via sublimation. The compound collects at the ends of the rotor, possibly due to cooling from the bearing gas which impinges on the rotor at the points where **1** condenses (see Fig. 5, II).

The ability to observe the sublimation behavior of **1** is an interesting consequence of the inhomogeneity in $H_{1\mathrm{H}}$. From a practical point of view, the sublimation behavior of **1** places a minor limitation on its use for chemical-shift referencing and for the determination of $H_{1\mathrm{H}}$ field strengths. It was found that the rate with which **1** accumulates at the ends of the rotor decreases when the rotor is packed tightly as was the case for the experiments shown in Fig. 5. But even when the material is packed loosely, the sublimation of **1** becomes a problem only if the ^{19}F resonance of **1** is used for chemical-shift referencing and field strength determinations several hours after the experiment is started. This is usually not a restriction since the ^{19}F resonance of **1** is visible in the spectrum after one transient. For long-term experiments that involve measurements at several different proton-decoupling field strengths, one can, after initially referencing with **1,** use any peak in the spectrum as a secondary reference. One can also avoid the problems arising from sublimation of **1** by mixing only some of the sample with **1** and packing this material in the center region of the rotor where $\gamma_{\mathrm{H}} H_{1\mathrm{H}}$ is within 10% of $\gamma_{\mathrm{H}} H_{1\mathrm{H\,max}}$. The rest of the rotor is filled with neat sample. A disk of weighing paper of the same diameter as the inner diameter of the rotor, placed at both interfaces of mixture and neat sample, effectively stops the sublimation of **1** out of the center region of the rotor.

(e) The Influence of the Proton-Decoupling Duty Cycle on the H_{1H} Field Strength

The proton-decoupling duty cycle is an important experimental parameter in quantitative [^{1}H]^{19}F NMR spectroscopy. In experiments that involve only a few transients, it was observed that the Bloch–Siegert shift decreases as the proton-decoupling duty cycle increases (data not shown). For a given proton-decoupling duty cycle, the Bloch–Siegert shift and the H_{1H} amplitude decrease as more and more scans are acquired until a plateau value is reached. This behavior is shown in Fig. 6 for the resonance of **1.** A rationale for these observations is that high-power proton decoupling leads to an increase in the coil circuitry temperature relative to typical probe-tuning conditions and thereby causes a reduction in performance. After a number of scans, thermal equilibrium is reached. The amplitude of the equilibrium $H_{1\mathrm{H}}$ field for a given RF input and the rate at which this equilibrium is reached depend on the decoupling duty cycle. The data shown in Fig. 6 were acquired with a duration of the proton pulse of 20.5 ms and a 4 s recycle delay. The equilibrium $H_{1\mathrm{H}}$ field strength which was reached after about 40 transients is 113 kHz, 4% less than the observed field amplitude after the first scan, 118 kHz.

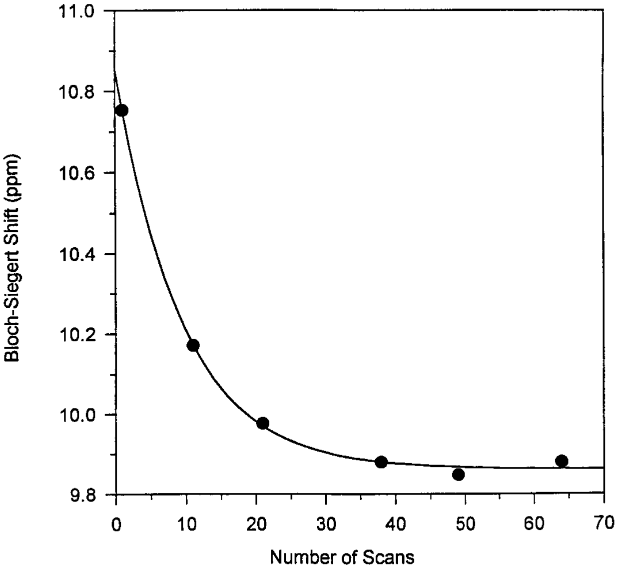

FIG. 6. Plot of the Bloch–Siegert shift of **1** as a function of the number of transients, in a [^{1}H]^{19}F MAS NMR experiment. The data were recorded using buffered acquisition. The proton pulse length was 20.5 ms, and the recycle delay was 4 s.

The observed effect possibly could be due to a temperature dependence of the ^{19}F chemical shift of **1.** To investigate this possibility, heating pulses were applied on the proton RF channel prior to the fluorine-excitation pulse. The proton-coupled ^{19}F chemical shift measured with and without heating pulses were identical. These data prove that the dependence of the Bloch–Siegert shift on the proton RF duty cycle is not due to a temperature dependence of the ^{19}F chemical shift of **1.**

Experimentally, different T_2 relaxation times for various samples require different ^{19}F acquisition times and different proton-decoupling pulse lengths. The influence of the decoupling duty cycle on the $H_{1\mathrm{H}}$ field strength means that the experimental protocol should involve a sufficient number of discarded scans prior to acquisition of the desired spectrum so that the coil circuit can reach thermal equilibrium. Second, the value of the $H_{1\mathrm{H}}$ field strength needs to be redetermined when the duty cycle of the proton decoupling is changed. These considerations are of little concern when routine [^{1}H]^{19}F NMR spectra are acquired. They are important when it is necessary to know the $H_{1\mathrm{H}}$ field amplitude and when it is important that the field strength remains constant throughout the experiment. A procedure for tuning and matching of the proton RF coil circuit under measurement conditions is described below.

(f) Tuning and Matching of the ^{1}H RF Coil Circuitry under Measurement Conditions

In some of our [^{1}H]^{19}F solid-state NMR experiments, proton-decoupling fields as large as 158 kHz were employed. As the proton amplifier was used at higher and higher power levels, an increasingly severe loss of signal-to-noise at the fluorine observe frequency (94.2 MHz) occurred. This S/N loss was traced to the proton frequency synthesizer that was producing a small 94 MHz artifact. In the extreme case, the ‘‘contamination’’ of the frequency synthesizer led to overloading of the receiver. Significant improvements in the signal-to-noise ratio were achieved by using RF filters designed to eliminate the ^{19}F frequency from the signal coming out of the high-power proton amplifier. Use of these RF filters leads to a 1 dB attenuation of the proton RF voltage measured at the probe. Importantly, it was found that the proton field strengths measured when using these RF filters were reduced by 10–20% compared to experiments not using the filters, but at the same probe RF voltage. The reason for this difference is that the impedance of the RF circuit is changed by insertion of the filters, and this change is not compensated for in our routine tuning procedure. This tuning and matching procedure involves sending a low-power signal into the circuit and then adjusting the tuning and matching capacitors to give minimum power reflection. This procedure does not simulate the same conditions under which the actual experiment is performed since the RF filters that are used in the experiment are not in the tuning circuit. Furthermore, the impedance of electronic components in the circuit changes with temperature (see previous section) which in turn is sensitive to the power levels and the duty cycles employed. An on-line tuning procedure that is implemented under actual measurement conditions eliminates these shortcomings. The performance of the circuit is optimized by adjusting the tuning and matching capacitors while the electronic components of the circuit are at their actual operating temperature, i.e., the equilibrium temperature of the circuit for a given decoupling duty cycle.

A convenient way to accomplish on-line tuning in proton-dipolar-decoupled ^{19}F MAS NMR uses the Bloch–Siegert shift. One-scan [^{1}H]^{19}F spectra were taken of **1** (see under Experimental). The tune and match capacitors of the proton RF channel are adjusted while the frequency of the ^{19}F resonance is monitored. Improvements in the coil performance are observed as an upfield shift of the ^{19}F resonance of **1** since an optimized tune leads to greater $H_{1\mathrm{H}}$ field and thus a greater Bloch–Siegert shift. This method is a fast way to obtain optimum performance of the probe’s ^{1}H RF circuitry under actual measurement conditions.

The applications of the Bloch–Siegert shift presented in this paper are not limited to [^{1}H]^{19}F MAS NMR spectroscopy. Double-resonance experiments involving two nuclei with similar Larmor frequencies can show significant Bloch–Siegert shifts, depending on the H_1 amplitudes employed (Eqs. [1] and [2]). For example, in ^{15}N-decoupled ^{13}C NMR experiments at 2.35 T, a decoupling field amplitude of 30 kHz (69.5 G) gives rise to a Bloch–Siegert shift of 10.4 ppm (263 Hz). [^{19}F]^{1}H MAS NMR spectroscopy is another example in which the Bloch–Siegert shift is a useful tool. In this case, the Bloch–Siegert shift is comparable to the range of proton chemical shifts.

CONCLUSIONS

Bloch–Siegert shifts in [^{1}H]^{19}F MAS NMR spectroscopy need to be considered when citing fluorine chemical shifts. A simple way to obtain ^{19}F chemical shifts independent of proton field is by setting the fluorine resonance of an internal reference material, e.g., **1,** to its proton-coupled ^{19}F chemical-shift value. The measurement of Bloch–Siegert shifts provides the experimental data to directly evaluate the amplitude of the proton H_1 field and the extent of its inhomogeneity throughout the sample volume. The impact of the inhomogeneity in $H_{1\mathrm{H}}$ is experiment dependent. In [^{1}H]^{19}F NMR experiments, the inhomogeneity in the proton-decoupling field is usually not visible as distortions in the lineshapes since linewidths at half-height of $\approx$1 kHz are typical. However, even in such experiments, the portion of the sample that is packed at the ends of the rotor experiences insufficient proton decoupling if the entire rotor volume is used. The ^{19}F RF field amplitude profile will show a position dependence analogous to the $H_{1\mathrm{H}}$ amplitude. If a ^{19}F pulse is applied that corresponds to a 90° rotation for ^{19}F spins in the center of the rotor, the excitation of the ^{19}F spins at either end of the rotor can be much less (a 23° tip angle for the probe used in this study). Measurements of spin–lattice relaxation times in the rotating frame, $T_{1\rho}$(^{1}H) or $T_{1\rho}$(^{19}F), can give drastically different results for samples that are packed in the middle third of the rotor versus samples that are packed in an outer third of the rotor. If the entire rotor is filled with sample, the observed relaxation time is an average over the range of the different H_1 field amplitudes.

The Bloch–Siegert shift has proven to be a sensitive monitor of the temperature-dependent electronic performance of standard solid-state NMR probes. Characterization of this dependence may be important in many rotating-frame relaxation-time measurements and in variable-temperature NMR studies. The measurement of the Bloch–Siegert shift also provides a convenient way to tune and match the proton RF circuit in the probe under actual measurement conditions, thereby optimizing the impedance of the circuit at its operating temperature and also taking into account the effect that RF filters may have on the impedance.

ACKNOWLEDGMENTS

The author gratefully thanks Dr. Edward W. Hagaman (Oak Ridge National Laboratory, Division of Chemical and Analytical Sciences) for his support and many helpful discussions concerning this work. The author further thanks Professor Kurt Zilm, Yale University, for valuable discussions on the Bloch–Siegert shift and its formal expression as shown in Eqs. [1] and [2]. This research was supported by the Division of Chemical and Analytical Sciences, Office of Basic Energy Sciences, U.S. Department of Energy, under Contract DE-AC05-840R21400 with Martin Marietta Energy Systems, Inc., and in part by an appointment of S.A.V. to the Oak Ridge National Laboratory Postdoctoral Research Associates Program administered jointly by the Oak Ridge Institute for Science and Education and Oak Ridge National Laboratory.

REFERENCES

1. F. Bloch and A. Siegert, *Phys. Rev.* **57,** 552 (1940).
2. M. Mehring, ''High Resolution NMR Spectroscopy in Solids in NMR—Basic Principles and Progress'' (P. Diehl, E. Fluck, and R. Kosfeld, Eds.), p. 225, Springer-Verlag, Berlin/Heidelberg, 1976.
3. A. Abragam, ''Principles of Nuclear Magnetism,'' p. 21, Oxford Univ. Press, Oxford, 1986.
4. G. G. Webb, dissertation, Yale University, 1988.
5. M. C. Leifer, *J. Magn. Reson. A* **105,** 1 (1993).
6. G. A. Olah, J. T. Welch, Y. D. Vankar, M. Nojima, I. Kerekes, and J. A. Olah, *J. Org. Chem.* **44,** 3872 (1979).
7. W. Adcock and N. A. Trout, *J. Org. Chem.* **56,** 3229 (1991).
8. W. Adcock and G. B. Kok, *J. Org. Chem.* **52,** 356 (1987).
9. E. W. Hagaman and S. K. Lee, *Energy Fuels* **9,** 729 (1995).
10. E. O. Stejskal and J. Schaefer, *J. Magn. Reson.* **28,** 105 (1977).